Journal of Alloys and Compounds 480 (2009) 981–986

Contents lists available at ScienceDirect

Journal of Alloys and Compounds

journal homepage: www.elsevier.com/locate/jallcom

Sputtered Al-doped lithium manganese oxide films for the cathode of lithium ion battery: The post-deposition annealing temperature effect

Y. Zhang[a], L.Z. Ouyang[a], C.Y. Chung[b], M. Zhu[a,*]

[a] School of Mechanical Engineering, South China University of Technology, Guangzhou 510640, PR China
[b] Department of Physics and Materials Science, City University of Hong Kong, Hong Kong, PR China

ARTICLE INFO

Article history:
Received 20 November 2008
Received in revised form 23 February 2009
Accepted 24 February 2009
Available online 9 March 2009

Keywords:
Lithium ion battery
Lithium manganese oxide
Thin film
Phase equilibrium

ABSTRACT

In this paper, lithium-excess Al-doped lithium manganese oxide films were prepared by R.F. magnetron sputtering at ambient temperature. X-ray diffraction, scanning electron microscopy, Raman spectra and constant current charge/discharge cycling were employed to study the post-deposition annealing effect. It has been found that the annealing temperature threshold for a single spinel phase was about 600 °C in oxygen atmosphere. The films annealed at 500 °C showed a composite structure with fine particles, which resulted in good capacity retention capability in both 4 V and 3 V regions. When annealed at 700 °C, a lithium deficient phase appeared, which led to structure reorganization and reduced adhesion of the cathode films to underlying Pt films, which caused poorer capacity retention capability.

1. Introduction

Spinel $LiMn_2O_4$ has attracted significant attention as an alternative cathode material for lithium ion batteries in recent years because it is more cost-effective and environmentally benign than other lithium transition-metal oxides. However, $LiMn_2O_4$ suffers considerable capacity fading, especially at high temperature, when it is cycled with organic electrolyte, which prevents it from widespread commercial applications. Capacity fading mechanisms for $LiMn_2O_4$ has long been studied and the contributing factors discussed in the literature can be summarized as follows [1–7]: (a) electrolyte decomposition at high voltage region; (b) disproportion reaction of Mn^{3+} to Mn^{4+} and Mn^{2+}, in which Mn^{2+} may readily dissolve into electrolyte; (c) local Jahn–Teller distortion at high discharge rates; (d) structure failure in the two-phase (4.2 V) region and (e) oxygen defects.

The most common way to stabilize its structure and thereby improve its cycleability is by doping with metal ions such as Li^+ [8], La^+ [9], Ga^{3+} [10], Bi^{3+} [11], Al^{3+} [12,13] and Sn^{4+} [14]. The other approach is by surface modification with protective coatings including Al_2O_3 [15], ZnO [16], ZrO_2 [17] and SiO_2 [18]. Among all of the methods mentioned above, many researchers have reported that spinel $LiMn_2O_4$ with slight Al-doping showed better electrochemical properties than the pristine one [12,13]. The underlying mechanisms for this improvement are proposed as follows: (a) easy formation of $LiMn_{2-x}Al_xO_4$ solid solution because Al^{3+} has ionic radius (0.057 nm) closer to that of Mn^{3+} (0.066 nm); (b) stronger chemical bonding between Al^{3+} and oxygen ions, which prohibits dissolution of Mn ions into electrolyte solution and (c) suppression of Jahn–Teller distortion by reduction of Mn^{3+}. In addition, electrochemical properties of doped or pristine $LiMn_2O_4$ have also been reported to be dependent on its particle size, morphology and structure [6,8,12–14]. Therefore, $LiMn_2O_4$ prepared by different synthesis routes or precursors showed substantially different performance.

$LiMn_2O_4$ in thin film form, prepared by either PVD or solution-deriving methods [19–29], is widely considered as a promising cathode material for all-solid-state thin film battery, which can be used as an integrated and self-sustained power source for MEMS devices, micro-sensors, smart cards and nonvolatile memory chips. The electrochemical properties of thin $LiMn_2O_4$ film were found to vary significantly with preparation conditions. As a result, many attempts have been made to improve structural stability and cycleability of thin $LiMn_2O_4$ film by optimization of deposition parameters or doping. Recently, Li and Fu reported that addition of ZrO_2 to $LiMn_2O_4$ film could overcome the disadvantage of two distinct voltages in 3 V and 4 V regions [26]. Ogumi and co-workers reported that lithium-ion excess $Li_{1.03}Mn_{1.97}O_4$ thin film showed better capacity retention capability than the nearly stoichiometric $Li_{1.01}Mn_{1.99}O_4$ [7]. Chen et al. showed that oxygen plasma treatments significantly improved the electrochemical properties of $LiMn_2O_4$ thin films prepared by R.F. magnetron sputtering [30]. However, the effect of dual ions doping with lithium and Al on performance of thin $LiMn_2O_4$ film has rarely been studied so far.

* Corresponding author. Tel.: +86 20 87113924.
E-mail address: memzhu@scut.edu.cn (M. Zhu).

0925-8388/$ – see front matter © 2009 Elsevier B.V. All rights reserved.
doi:10.1016/j.jallcom.2009.02.116

In this work, lithium-excess Al-doped lithium manganese oxide films were prepared by R.F. magnetron sputtering and their structure and electrochemical performance was investigated as a function of post-annealing temperature.

2. Experimental details

The Φ60 mm targets for R.F. magnetron sputtering were made by cold-pressing and calcining mixture of $LiMn_{1.98}Al_{0.02}O_4$ and Li_2CO_3 (molar ratio: 0.075:1) at 850 °C for 6 h in air. $LiMn_{1.98}Al_{0.02}O_4$ was received from Great Power Battery Company, Guangzhou, China. Some of the targets were bonded to copper plates by thermal conducting Ag epoxy to enhance their mechanical strength and durability during ion bombardment. All film were deposited onto Pt metalized Si substrates (Pt (300 nm)/Ti (30 nm) SiO_2/Si) using a R.F. power of 70 W. The base pressure was typically below 10^{-5} Pa and the target-substrate distance was fixed to 6 cm. The processing gas was a mixture of Ar and O_2 with flow ratio of 3:1 and the processing pressure was set to 10 mTorr. Post-deposition annealing was carried out in an O_2-flowing tube furnace at 500 °C, 600 °C, 700 °C, especially, for 2 h.

The structure of as-deposited and annealed films was examined by X-ray diffraction with Cu-K radiation (Pillips X'pert plus) and Raman spectroscopy (Renishaw RM3000). The surface and cross-sectional morphology of as-prepared and cycled films were observed using a field-emission scanning electron microscope (LEO 1530VP). Films cycled 20 times were rinsed by acetone in glove box and dried in air prior to SEM observation. Charge and discharge cycles were performed in a home-made three-electrodes cell on Autolab PGSTAT 30 in an argon-filled glove box with the content of oxygen and moisture less than 2 ppm. Both the counter and reference electrode were lithium (battery grade). The electrolyte was 1 M $LiClO_4$ in propylene carbonate (PC) (battery grade, water content <30 ppm). Constant current for charge and discharge cycles was 10 $\mu A\,cm^{-2}$ in 4 V region (cutoff voltage: 3.4–4.3 V) and both 4 V and 3 V regions (cutoff voltage: 2.5–4.3 V).

3. Results and discussion

3.1. Morphology evolution

It can be inferred that as-deposited films were lithium-excess by combining the results of Raman spectra and initial charge voltage profiles of annealed films, as can be found later in the corresponding part. To avoid confusion, as-deposited films will be denoted as $Li_{1+\delta}Mn_{1.98}Al_{0.02}O_4$. Fig. 1 shows surface morphology evolution of $Li_{1+\delta}Mn_{1.98}Al_{0.02}O_4$ films before and after post-deposition annealing. As shown in Fig. 1(a), as-deposited $Li_{1+\delta}Mn_{1.98}Al_{0.02}O_4$ film was smooth and dense. These films are more featureless than those prepared at higher R.F. power density [26]. Therefore, lateral diffusion of impinging species on Pt metalized Si substrates could be more adequate in this case. One possible reason is that the deposition rate, about 5 nm/min in this work, was a little less than that reported by ref. [26] (7–8 nm/min). As we can see later, as-deposited $Li_{1+\delta}Mn_{1.98}Al_{0.02}O_4$ films were lithium-excess. Lithium is less loosely bonded in $LiMn_2O_4$ and thus the activation energy for lithium diffusion is much less than that of other strongly bonded ionic species. Thereby, the other possible reason is that more lithium was incorporated into the as-deposited films in this work than in Ref. [26]. And higher content of lithium species contributes to more adequate lateral diffusion. After post-deposition annealing at 500 °C for 2 h, $Li_xMn_{1.98}Al_{0.02}O_4$ films exhibit a granular morphology with a very fine and uniform particle size of less than 100 nm. A small amount of the debris was also observed on the surface. This can be seen more clearly in zoomed-out SEM images (not shown) and is believed to result from the crystallization of $Li_{1+\delta}Mn_{1.98}Al_{0.02}O_4$ films when subjected to annealing. As the annealing temperature increased to 600 °C, $Li_{1+\delta}Mn_{1.98}Al_{0.02}O_4$ film shows a granular morphology without any debris on the surface. Furthermore, larger particle agglomerates and inter-particle necking were observed, as shown in the inset of Fig. 1(c). It can be concluded that the particles grow upon annealing. As the annealing temperature further increased to 700 °C, the particle agglomerates coarsened slightly, whereas their feature size is still below 100 nm. Besides, a considerable amount of secondary particles with a well-defined shape and a feature size of several hundred nanometers were embedded in the films. These secondary particles could result from a phase transition triggered by high temperature annealing.

Cross-sectional morphology evolution of $Li_{1+\delta}Mn_{1.98}Al_{0.02}O_4$ films after post-deposition annealing was shown in Fig. 2. It can be seen that $Li_{1+\delta}Mn_{1.98}Al_{0.02}O_4$ films exhibited a dense fibrous structure after annealing at 500 °C. A loosely packed columnar structure

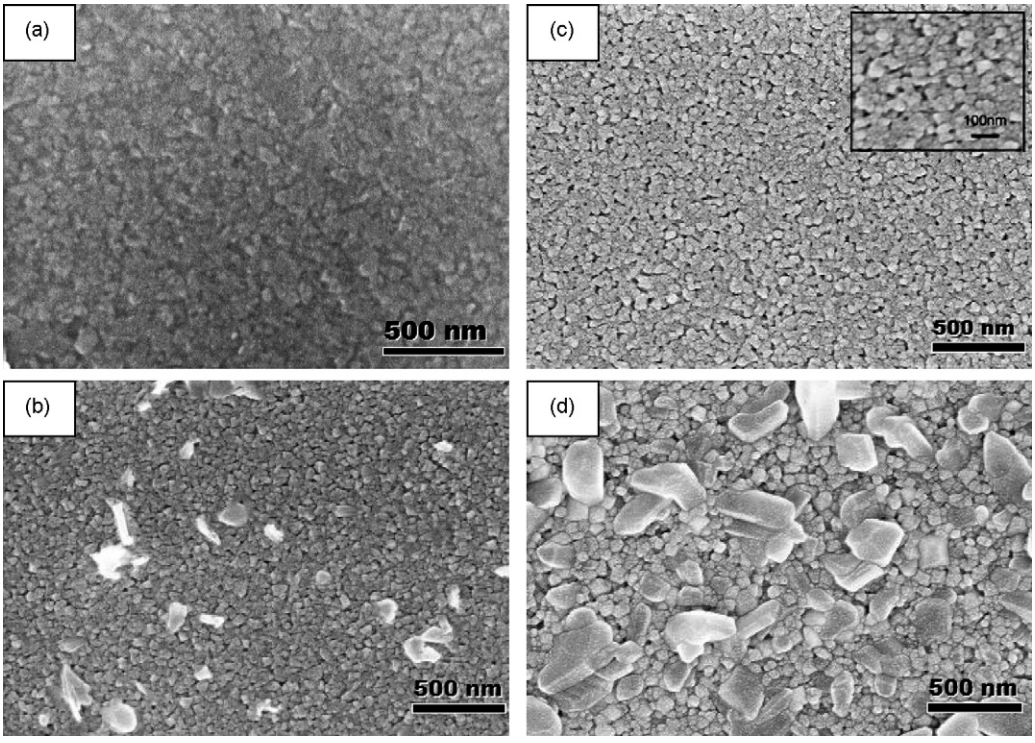

Fig. 1. Surface-view SEM images of $Li_{1+\delta}Mn_{1.98}Al_{0.02}O_4$ films: (a) as-deposited, (b) annealed at 500 °C, (c) annealed at 600 °C and (d) annealed at 700 °C. The inset in (c) shows its larger particle agglomerates and inter-particle necking.

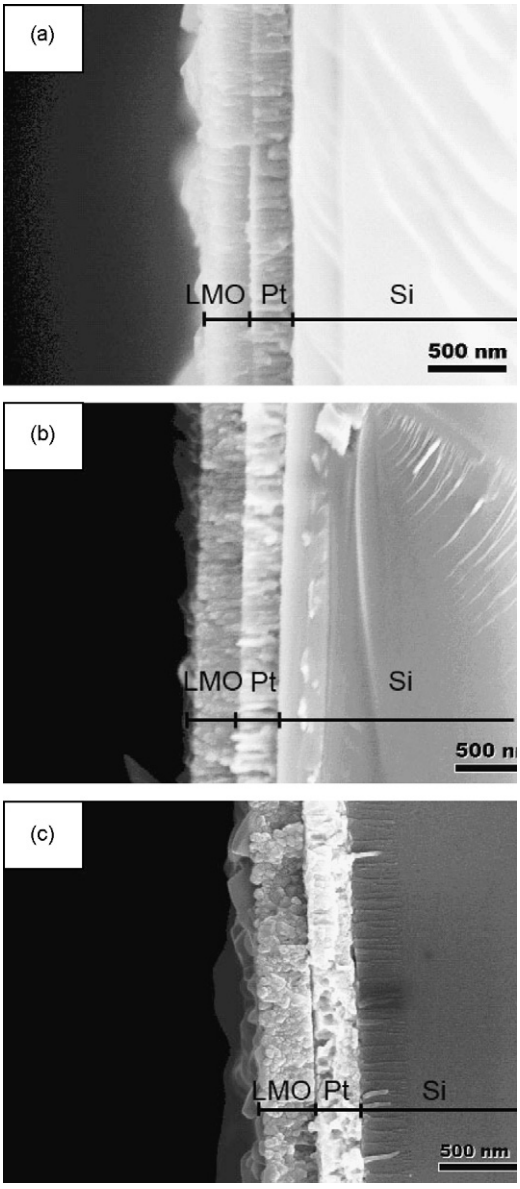

Fig. 2. Cross-sectional view of SEM images of $Li_{1+\delta}Mn_{1.98}Al_{0.02}O_4$ films: (a) annealed at 500 °C, (b) annealed at 600 °C and (c) annealed at 700 °C.

developed when the annealing temperature increased to 600 °C. After annealing at 700 °C, the microstructure of $Li_{1+\delta}Mn_{1.98}Al_{0.02}O_4$ films reorganized and an equiaxial crystal structure formed. These results are consistent with the surface morphology evolution. The driving force for grain coarsening should be minimization of as-deposited residual film stress and surface energy of the particles. It should be stressed that the adhesion between $Li_{1+\delta}Mn_{1.98}Al_{0.02}O_4$ films and underlying Pt metalized Si substrate becomes weaker as a result of structure reorganization after annealing at 700 °C.

3.2. Structure characterization

As-deposited $Li_{1+\delta}Mn_{1.98}Al_{0.02}O_4$ films were confirmed to have an X-ray amorphous structure (not shown), which is consistent with other results on pristine $LiMn_2O_4$ films. Fig. 3 shows the powder X-ray diffraction patterns of $Li_{1+\delta}Mn_{1.98}Al_{0.02}O_4$ films annealed at 500 °C, 600 °C and 700 °C, respectively. Besides peaks from the substrates, one broadened peak at 18.63° and the other at 32.38° were found for the $Li_{1+\delta}Mn_{1.98}Al_{0.02}O_4$ films annealed at 500 °C. The former can be ascribed to (1 1 1) peak of spinel $LiMn_2O_4$ phase. The

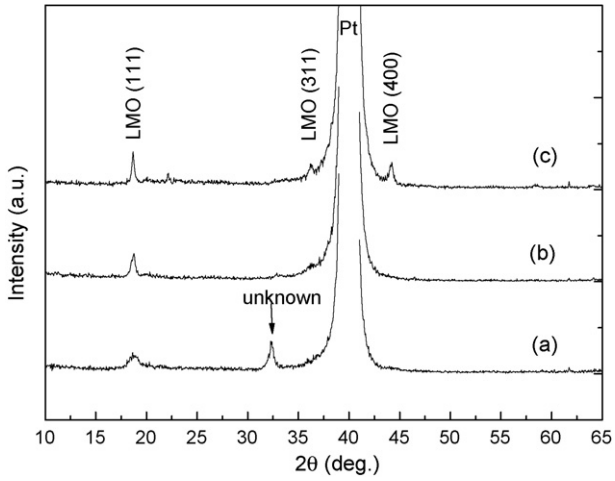

Fig. 3. X-ray diffraction patterns of $Li_{1+\delta}Mn_{1.98}Al_{0.02}O_4$ films annealed at 500 °C (a), 600 °C (b) and 700 °C (c). (LMO is referred to as spinel $LiMn_2O_4$ phase. The arrow shows an unknown peak from annealed $Li_{1+\delta}Mn_{1.98}Al_{0.02}O_4$ film at 500 °C.)

latter could be due to the other phase and will be discussed later. When the annealing temperature elevated to 600 °C, peak (1 1 1) became sharper and peak (3 1 1) also appeared. Peaks (1 1 1) and (3 1 1) were even sharper and peak (4 0 0) emerged as the annealing temperature increased to 700 °C. It can be concluded that crystallinity of $Li_{1+\delta}Mn_{1.98}Al_{0.02}O_4$ films was improved as the annealing temperature increased because the higher the annealing temperature, the narrower the reflection peaks. Typical sputtered and annealed films, like $LiCoO_2$, are highly textured as a result of residual stress imparted by the sputter deposition process. (1 1 1) texture may exist in the $Li_{1+\delta}Mn_{1.98}Al_{0.02}O_4$ films annealed at 500 °C since no peaks other than (1 1 1) were found. Apart from nano-sized particle, which can be readily discerned from the SEM morphology in Fig. 1(b), the residual stress may also contribute to the broadening of peak (1 1 1). When annealed at 600 °C, both (3 1 1) and (1 1 1) reflections can be discerned, which means no strong preferred orientation existed any more. After annealing at 700 °C, the structure of $Li_{1+\delta}Mn_{1.98}Al_{0.02}O_4$ films reorganized as a consequence of minimization of as-deposited residual film stress and surface energy of the particles. As a result, there is no preferred orientation in films annealed at 700 °C.

Fig. 4 shows Raman spectroscopy of $Li_{1+\delta}Mn_{1.98}Al_{0.02}O_4$ films annealed at 500 °C, 600 °C and 700 °C, respectively. According to

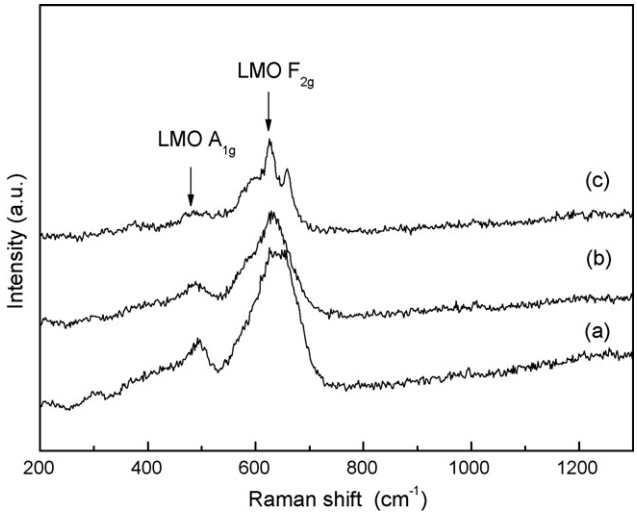

Fig. 4. Raman spectra of $Li_{1+\delta}Mn_{1.98}Al_{0.02}O_4$ films annealed at 500 °C (a), 600 °C (b) and 700 °C (c). (LMO is referred to as spinel $LiMn_2O_4$ phase.)

the factor group theory, Raman spectra of spinel $LiMn_2O_4$ have five characteristic modes ($A_{1g} + E_g + 3F_{2g}$) [23]. These five modes result from the localized vibration of MnO_6 octahedra and LiO_4 tetrahedra. For $Li_{1+\delta}Mn_{1.98}Al_{0.02}O_4$ films annealed at 500 °C, two Raman peaks, at 640 cm^{-1} and 495 cm^{-1}, appeared. The 640 cm^{-1} peak represents the A_{1g} Mn–O stretching vibration mode and the 495 cm^{-1} peak corresponds to $F_{2g}^{(2)}$ vibration mode. As we can see from Fig. 4(a), the 640 cm^{-1} peak was asymmetric and significantly broadened. It may be composed of several overlapping peaks. By comparison with Raman spectra of $LiMn_2O_4$, $Li_2Mn_2O_4$ and $LiMnO_2$, the broadened 640 cm^{-1} might be resulted from the coexistence of these three phase: $LiMn(Al)_2O_4$, $Li_2Mn(Al)_2O_4$ and $LiMn(Al)O_2$, in which the doped Al can be assumed to equally locate in the Mn sites of these phase and will be denoted as Mn(Al) in the rest of this manuscript. The extra X-ray reflection at 32.38° of $Li_{1+\delta}Mn_{1.98}Al_{0.02}O_4$ films annealed at 500 °C might be caused by $Li_2Mn(Al)_2O_4$ or $LiMn(Al)O_2$. Due to the coexistence of the above-mentioned phases, the average Li/Mn ratio of films annealed at 500 °C should be more than 1:2. It can be seen that films annealed at 500 °C were lithium-rich, and therefore, the same were the as-deposited films. As-deposited $Li_{1+\delta}Mn_{1.98}Al_{0.02}O_4$ films were homogenous and had an amorphous structure. After 500 °C annealing, as-deposited films crystallized and decomposed into two phases, one spinel $LiMn(Al)_2O_4$ and one lithium rich, $Li_2Mn(Al)_2O_4$ or $LiMn(Al)O_2$. During the process of crystallization and decomposition, it is likely that a small amount of lithium species was evaporated. As mentioned above, there was a small amount of debris on the surface of $Li_{1+\delta}Mn_{1.98}Al_{0.02}O_4$ films annealed at 500 °C. These debris might due to interfacial reaction of evaporated lithium species with residual CO_2 in the tube furnace and, therefore, they might be Li_2CO_3. After annealing at 600 °C, the A_{1g} mode shifted to 634 cm^{-1} and became narrower. This means that the amount of unstable $Li_2Mn(Al)_2O_4$ and $LiMn(Al)O_2$ phase greatly decreased. However, the A_{1g} mode was splitted into two peaks, one at 629 cm^{-1} and the other at 660 cm^{-1} after at 700 °C. Similar phenomenon was also observed in pristine $LiMn_2O_4$ films annealed at high temperature and is believed to result from a cationic disorder in the Mn–O framework [23]. This can be interpreted by phase mixing of spinel $LiMn_2O_4$ and lithium deficient manganese oxide, possibly $Mn(Al)O_2$ or $Mn(Al)_3O_4$, which means that the films annealing at 700 °C were lithium deficient. By comparing the phase structure of films annealing at different temperatures, it can be found that lithium content decreased as the temperature increased.

3.3. Electrochemical performance

The constant charge and discharge curves of $Li_{1+\delta}Mn_{1.98}Al_{0.02}O_4$ films annealed at 500 °C, 600 °C and 700 °C were shown in Fig. 5. Apart from two sloped voltage plateaus at about 4 V, there was a short charge plateau at 2.95 V and a short sloped charge plateau at about 3.75 V for of $Li_{1+\delta}Mn_{1.98}Al_{0.02}O_4$ films annealed at 500 °C. When annealed at 600 °C, $Li_{1+\delta}Mn_{1.98}Al_{0.02}O_4$ films show well-defined voltage plateaus at both 3 V and 4 V regions, which is the fingerprint of spinel $LiMn_2O_4$. Furthermore, they show the largest capacity in both 4 V and 3 V regions and the polarization was also reduced. As the annealing temperature was further increased to 700 °C, the characteristic plateaus of spinel $LiMn_2O_4$ remained while the capacity in both 4 V and 3 V regions decreased. It is noted that the open circuit voltage of as-annealed $Li_{1+\delta}Mn_{1.98}Al_{0.02}O_4$ increased with annealing temperature. This indicates that the composition of $Li_{1+\delta}Mn_{1.98}Al_{0.02}O_4$ films changed after subjected to post-deposition annealing. The voltage plateau at 2.95 V is the feature of tetragonal $Li_2Mn_2O_4$ and the sloped plateau at 3.75 V should be due to layered $LiMn(Al)O_2$. These results are consistent with the conclusion drawn from the Raman spectra that $Li_{1+\delta}Mn_{1.98}Al_{0.02}O_4$ films annealed at 500 °C were lithium-excess and composed of

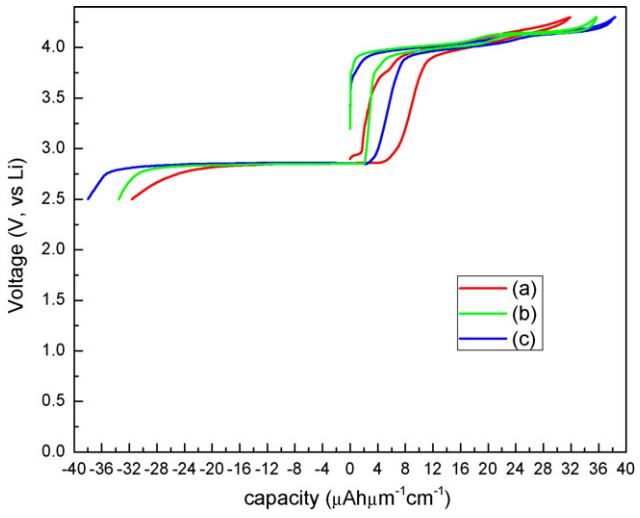

Fig. 5. The initial constant current charge and discharge voltage profiles of $Li_{1+\delta}Mn_{1.98}Al_{0.02}O_4$ films annealed at 500 °C (a), 600 °C (b) and 700 °C (c).

three phases: $LiMn(Al)_2O_4$, $Li_2Mn(Al)_2O_4$ and $LiMn(Al)O_2$, in which spinel $LiMn(Al)_2O_4$ was dominated. Due to poor crystallinity of $Li_{1+\delta}Mn_{1.98}Al_{0.02}O_4$ films annealed at 500 °C, there existed a significant polarization as can be seen from the gap between charge

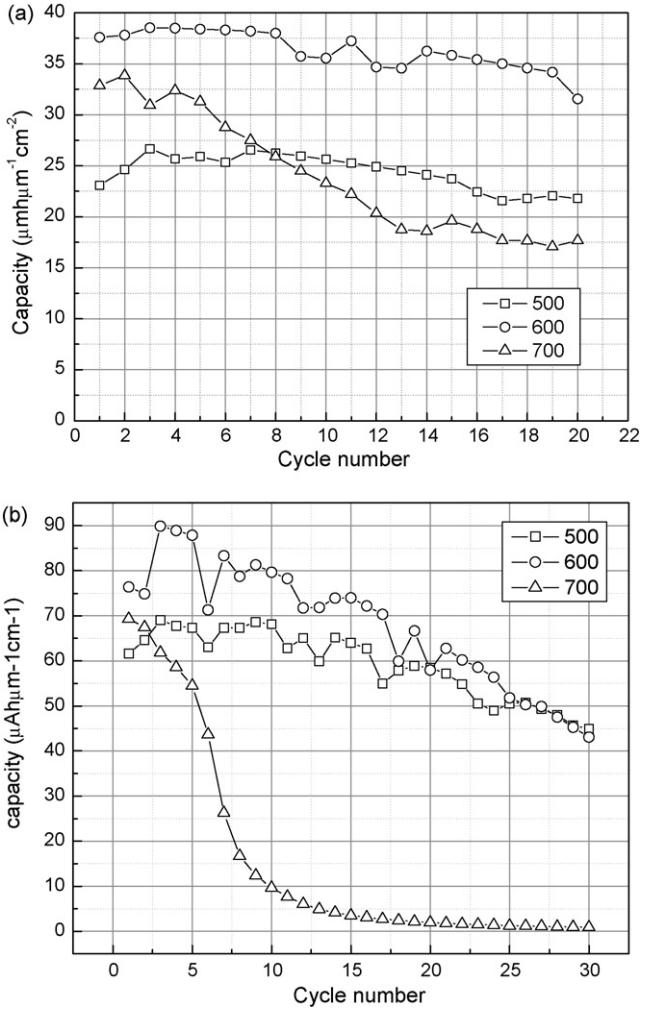

Fig. 6. Capacity vs cycle number plot of $Li_{1+\delta}Mn_{1.98}Al_{0.02}O_4$ films annealed at 500 °C, 600 °C and 700 °C in 4 V region (a) and in both 4 V and 3 V regions (b).

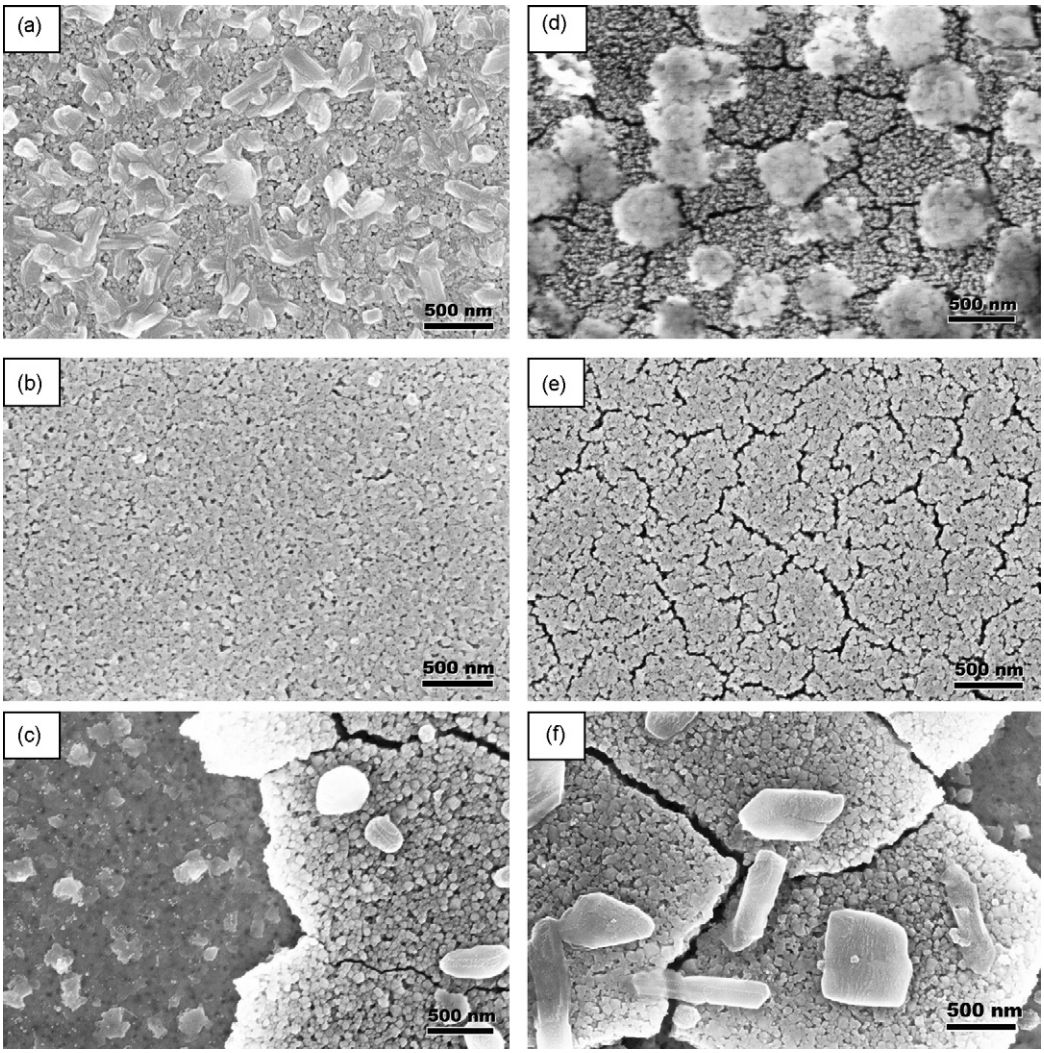

Fig. 7. Surface-view SEM images of $Li_{1+\delta}Mn_{1.98}Al_{0.02}O_4$ films cycled in 4 V region for 20 times after annealed at 500 °C (a), 600 °C (b) and 700 °C (c) and those cycled in both 4 V and 3 V regions for 20 times after annealing at 500 °C (d), 600 °C (e) and 700 °C (f).

and discharge curves. After 600 °C annealing, the composition of $Li_{1+\delta}Mn_{1.98}Al_{0.02}O_4$ films may be close to that of stoichiometric spinel $LiMn_{1.98}Al_{0.02}O_4$, for it shows characteristic charge and discharge voltage profile of spinel $LiMn_2O_4$. Lithium deficient may exist in $Li_{1+\delta}Mn_{1.98}Al_{0.02}O_4$ films annealed at 700 °C because it had a higher OCV (open circuit voltage) and less capacity than those annealed at 600 °C. This is consistent with the results obtained by SEM and Raman spectra that a second phase, possibly $Mn(Al)O_2$ or $Mn(Al)_3O_4$, was formed. $Li_{1+\delta}Mn_{1.98}Al_{0.02}O_4$ films annealed at 700 °C besides the spinel phase.

3.4. Capacity fading upon cycling

When cycled only in 4 V region, $Li_{1+\delta}Mn_{1.98}Al_{0.02}O_4$ films annealed at 600 °C exhibited the highest capacity ($38\ \mu Ah\ cm^{-2}\ \mu m^{-1}$) combined with reasonable capacity retention capability, as can be seen in Fig. 6(a). However, $Li_{1+\delta}Mn_{1.98}Al_{0.02}O_4$ films annealed at 500 °C showed better capacity retention capability, although their initial discharge capacity was as low as $23\ \mu Ah\ cm^{-2}\ \mu m^{-1}$. When annealing temperature increased to 700 °C, the capacity of $Li_{1+\delta}Mn_{1.98}Al_{0.02}O_4$ films decreased and degraded very fast. Good retention capability of $Li_{1+\delta}Mn_{1.98}Al_{0.02}O_4$ films annealed at 500 °C may result from the fact that they had a composite structure with fine particles. It was also observed that a lot of precipitates formed on the surface of cycled $Li_{1+\delta}Mn_{1.98}Al_{0.02}O_4$ films annealed at 500 °C (Fig. 7(a)). Those precipitates could be due to the interfacial reaction between lithium-excess $Li_{1+\delta}Mn_{1.98}Al_{0.02}O_4$ films and the liquid organic electrolyte solution. The precipitates may contribute to capacity retention capability by acting as a protective layer and preventing further side reactions that is commonly observed for spinel $LiMn_2O_4$ [7]. By comparing the surface morphology change before (Fig. 1(b)) and after 600 °C (Fig. 7(b)) annealing, it can be seen that surfaces of the cycled films were smoother and more featureless. Therefore, capacity fading mechanism of $Li_{1+\delta}Mn_{1.98}Al_{0.02}O_4$ films annealed at 600 °C could be the same as that of pristine spinel $LiMn_2O_4$, for which Mn dissolves into the liquid electrolyte as a result of disproportion reaction ($2Mn^{3+} \rightarrow Mn^{4+} + Mn^{2+}$). The $Li_{1+\delta}Mn_{1.98}Al_{0.02}O_4$ films annealed at 700 °C cracked and peeled off after cycling, as shown in Fig. 7(c). This is believed to be caused by the poor adhesion between the films and underlying Pt films as a sequence of structure reorganization and particle coarsening. As a consequence, the capacity of $Li_{1+\delta}Mn_{1.98}Al_{0.02}O_4$ films annealed at 700 °C degraded very fast.

When the cutoff voltage extended to 3 V region (2.5–4.3 V), the capacity of annealed $Li_{1+\delta}Mn_{1.98}Al_{0.02}O_4$ films was doubled, as shown in Fig. 6(b). However, their capacity fading was much more severe. Cracks were formed on the surface of cycled $Li_{1+\delta}Mn_{1.98}Al_{0.02}O_4$ films and should be caused by Jahn–Teller distortion, the phase transition from cubic phase to tetragonal phase

with large volume change. It can be concluded that very small amount of Al doping ($LiMn_{1.98}Al_{0.02}O_4$) cannot prohibit Jahn–Teller distortion at room temperature. But further investigation is needed to address the Al-doping effect by varying the Al doping content. $Li_{1+\delta}Mn_{1.98}Al_{0.02}O_4$ films annealed at 500 °C showed the best capacity retention capability in the extended voltage window. The reason could be the same as proposed above that they had a composite structure with fine particles and a thicker passive layer formed on their surface acted as a protective layer. It is interesting that the morphology of the precipitates varied greatly when the cutoff voltage extended to 3 V region for $Li_{1+\delta}Mn_{1.98}Al_{0.02}O_4$ films annealed at 500 °C. The detailed chemistry and formation mechanism of these precipitates need to be further investigated. Similar to those cycled in only 4 V region, $Li_{1+\delta}Mn_{1.98}Al_{0.02}O_4$ films annealed at 700 °C peeled off due to poor adhesion to the underlying Pt film when cycled in the broadened voltage window.

4. Conclusions

Lithium-excess $Li_{1+\delta}Mn_{1.98}Al_{0.02}O_4$ films were deposited by R.F. magnetron sputtering from a sintered $Li_{1.15}Mn_{1.98}Al_{0.02}O_4$ target. Post-deposition annealing temperature was shown to have a critical impact on the morphology, structure and electrochemical of $Li_{1+\delta}Mn_{1.98}Al_{0.02}O_4$ films. The particles in the deposited film coarsened when subjected to post-deposition annealing. When annealed at 500 °C, $Li_{1+\delta}Mn_{1.98}Al_{0.02}O_4$ films have a composite structure with fine particles, in which three phases, $LiMn(Al)_2O_4$, $Li_2Mn(Al)_2O_4$ and $LiMn(Al)O_2$, co-exited, and thus have very good capacity retention capability in both 4 V and 3 V regions. $Li_{1+\delta}Mn_{1.98}Al_{0.02}O_4$ films annealed at 600 °C showed a well-crystallized single-phase structure of stoichiometric spinel $LiMn_{1.98}Al_{0.02}O_4$ films and had higher discharge capacity. However, a lithium deficient phase, possibly $Mn(Al)O_2$ or $Mn(Al)_3O_4$, formed when annealing temperature was increased to 700 °C. This phase transition leaded to structure reorganization and reduced adhesion of the cathode films to underlying Pt films and thereby caused poorer capacity retention capability.

Acknowledgements

This work was supported by Ministry of Education (project no. IRT0551) and Natural Science Foundation of Guangdong Province under the Team Project.

References

[1] D. Aurbach, M.D. Levi, K. Gamulski, B. Markovsky, G. Salitra, E. Levi, U. Heider, L. Heider, R. Oesten, J. Power Sources 82 (1999) 472–479.
[2] Y. Xia, T. Sakai, T. Fujieda, X. Yang, X. Sun, Z. Ma, J. McBreen, M. Yoshio, J. Electrochem. Soc. 148 (2001) A723–A729.
[3] N. Terada, T. Yanagi, A. Arai, M. Yoshikawa, K. Ohta, N. Nakajima, A. Yanai, N. Arai, J. Power Sources 100 (2001) 80–92.
[4] X. Wang, H. Nakamura, M. Yoshio, J. Power Sources 110 (2002) 19–26.
[5] Y.J. Shin, A. Manthiram, J. Electrochem. Soc. 151 (2004) A204–A208.
[6] B. Deng, H. Nakamura, M. Yoshio, J. Power Sources 180 (2008) 864–868.
[7] T. Doi, M. Inaba, Y. Iriyama, T. Abe, Z. Ogumi, J. Electrochem. Soc. 155 (2008) A20–A23.
[8] Z.H. Chen, K. Amine, J. Electrochem. Soc. 153 (2006) A316–A320.
[9] D. Arumugam, G. Paruthimal Kalaignan, P. Manisankar, Solid State Ionics 179 (2008) 580–586.
[10] D.Q. Liu, Z.Z. He, X.Q. Liu, J. Alloys Compd. 440 (2007) 69–73.
[11] C.L. Tan, H.J. Zhou, W.S. Li, X.H. Hou, D.S. Lu, M.Q. Xu, Q.M. Huang, J. Power Sources 184 (2008) 408–413.
[12] L.F. Xiao, Y.Q. Zhao, Y.Y. Yang, Y.L. Cao, X.P. Ai, H.X. Yang, Electrochim. Acta 54 (2008) 545–550.
[13] R. Thirunakaran, A. Sivashanmugam, S. Gopukumar, C.W. Dunnill, D.H. Gregory, J. Phys. Chem. Solids 69 (2008) 2082–2090.
[14] S.H. Guo, S.C. Zhang, X.M. He, W.H. Pu, C.Y. Jiang, C.R. Wan, J. Electrochem. Soc. 155 (2008) A760–A763.
[15] S.W. Lee, K.S. Kim, H.S. Moon, H.J. Kim, B.W. Cho, W.I. Cho, J.B. Ju, J.W. Park, J. Power Sources 126 (2004) 150–155.
[16] J. Tu, X.B. Zhao, J. Xie, G.S. Cao, D.G. Zhuang, T.J. Zhu, J.P. Tu, J. Alloys Compd. 432 (2007) 313–317.
[17] S. Lim, J. Cho, Electrochem. Commun. 10 (2008) 1478–1481.
[18] D. Arumugam, G. Paruthimal Kalaignan, J. Electroanal. Chem. 624 (2008) 197–204.
[19] Y.J. Park, J.G. Kim, M.K. Kim, H.T. Chung, W.S. Um, M.H. Kim, H.G. Kim, J. Power Sources 76 (1998) 41–47.
[20] N.J. Dudney, J.B. Bates, R.A. Zuhr, S. Young, J.D. Robertson, H.P. Jun, S.A. Hackney, J. Electrochem. Soc. 146 (1999) 2455–2464.
[21] K.A. Striebel, A. Rougier, C.R. Horne, R.P. Reade, E.J. Cairns, J. Electrochem. Soc. 146 (1999) 4339–4347.
[22] M. Mohamedi, D. Takahashi, T. Uchiyama, T. Itoh, M. Nishizawa, I. Uchida, J. Power Sources 93 (2001) 93–103.
[23] K.F. Chiu, H.H. Hsiao, G.S. Chen, H.L. Liu, J.L. He, H.C. Lin, J. Electrochem. Soc. 151 (2004) A452–A455.
[24] X.M. Wu, X.H. Li, Z. Wang, Z.B. Xiao, J.B. Liu, W.B. Yan, Mater. Chem. Phys. 83 (2004) 78–81.
[25] F.Y. Shih, K.Z. Fung, J. Power Sources 159 (2006) 1370–1376.
[26] C.L. Li, Z.W. Fu, Electrochim. Acta 52 (2007) 6155–6164.
[27] S.B. Tang, H. Xia, M.O. Lai, L. Lu, J. Alloys Compd. 449 (2008) 322–325.
[28] A. Subramania, S.N. Karthick, N. Angayarkanni, Thin Solid Films 516 (2008) 8295–8298.
[29] J. Xie, T. Tanaka, N. Imanishi, T. Matsumura, A. Hirano, Y. Takeda, O. Yamamoto, J. Power Sources 180 (2008) 576–581.
[30] C.C. Chen, K.F. Chiu, K.M. Lin, H.C. Lin, C.R. Yang, F.M. Wang, Phys. Scr. T129 (2007) 74–79.